Research Square

Preprints are preliminary reports that have not undergone peer review.
They should not be considered conclusive, used to inform clinical practice,
or referenced by the media as validated information.

Facile Hydrothermal Synthesis of Ag/C Submicron Wires Derived from Waste Cotton: Core/Shell Synergy for Enhanced Methylene Blue Adsorption

Hung-Bin Lee
National Taiwan Ocean University
Yu-Wei Tseng
National Taiwan Ocean University
Ming-Yuan Lin
Army Academy ROC
Ming-Chih Kuo
gmz@ulive.pccu.edu.tw

Chinese Culture University https://orcid.org/0009-0006-1864-4164

Research Article

Keywords: Hydrothermal carbonization, Carbon-based materials, Silver/carbon composites, Dye adsorption, Methylene blue, Adsorption kinetics

Posted Date: April 21st, 2026

DOI: https://doi.org/10.21203/rs.3.rs-9258938/v1

License: This work is licensed under a Creative Commons Attribution 4.0 International License.
Read Full License

Abstract

To address the challenge of textile waste upcycling, this study demonstrates a sustainable, acid-assisted hydrothermal strategy to transform waste cotton fibers into high-value functional carbon materials. By tuning reaction kinetics, we achieved the controlled synthesis of uniform submicron carbon spheres at 180°C for 4 h and novel silver/carbon (Ag/C) submicron wires by extending the process to 7 h. Morphological and structural analyses, including SEM, TEM, and SAED, confirm that the Ag/C composites possess a unique core/sheath architecture featuring quasi-single-crystalline silver cores encapsulated within a graphitized carbon matrix. Surface analysis via XPS and FT-IR reveals that strong interfacial interactions and a high density of oxygen- and sulfur-containing functional groups contribute to the material's enhanced surface reactivity. Performance benchmarks in methylene blue remediation show that the Ag/C submicron wires significantly outperform pristine carbon spheres in both adsorption kinetics and removal capacity, driven by the synergistic effect between the silver core and the functionalized carbon shell. These results highlight a robust and scalable pathway for engineering high-performance adsorbents from low-value textile waste for advanced environmental remediation.

Introduction

The rapid expansion of the global textile industry has led to a continuous increase in the production and consumption of cotton-based textiles. It is estimated that more than 24 million tons of cotton textile waste are generated annually worldwide, mainly from manufacturing offcuts and post-consumer garments (Kalabek et al. 2016). Currently, landfilling and incineration remain the dominant disposal routes, resulting in the loss of valuable resources and causing environmental problems such as land occupation, air pollution, and greenhouse gas emissions (Kalabek et al. 2016). Cotton waste is rich in cellulose, a renewable and carbon-rich biopolymer with inherent biodegradability. Its efficient conversion into functional carbon materials is therefore of great interest for developing sustainable materials and promoting circular resource utilization (Muhlack et al. 2018).

Recycling cotton textile waste is challenging due to its complex composition and mixed additives. Mechanical recycling often damages polymer chains, leading to inferior fiber strength and quality, whereas chemical recycling requires large quantities of solvents and energy, increasing both cost and environmental risk. Moreover, residual dyes, softeners, and finishing agents further hinder efficient recycling. Consequently, the development of environmentally friendly and economically viable conversion strategies remains a research hotspot in textile waste valorization (Anžlovar et al. 2022; Acharya et al. 2021).

Hydrothermal carbonization (HTC) has emerged as an effective method for converting biomass into carbonaceous materials under relatively mild conditions (Sharma et al. 2020; Cao et al. 2021; Peng et al. 2023). By mimicking natural geological processes in hot compressed water, HTC promotes dehydration, condensation, and aromatization reactions of carbohydrates, yielding a solid carbon-rich product known as hydrochar (Paksung et al. 2020). Importantly, HTC allows control over microstructure and surface

chemistry through reaction temperature (Ahn et al. 2024), time, and acidity, making it particularly attractive for tailoring functional carbon materials for adsorption, catalysis, and electrochemical applications (Basso 2016; Qi et al. 2016).

Under natural conditions, hydrothermal reactions have long governed the geological evolution of organic matter into coal and petroleum. By mimicking this process in the laboratory through hydrothermal treatment, rapid carbonization of biomass can be achieved within only a few hours. For cotton fibers, the main constituent cellulose is a high-molecular-weight polysaccharide composed of β-1,4-glycosidically linked glucose units and contains abundant hydroxyl functional groups, making it highly susceptible to hydrolysis under acidic environments. In the presence of sulfuric acid, cellulose is first catalytically hydrolyzed into glucose, which is subsequently dehydrated to form 5-hydroxymethylfurfural (HMF). The HMF molecules exhibit high chemical reactivity and can undergo further condensation and polymerization reactions under hydrothermal conditions to form carbonaceous precursors. With increasing reaction time, these precursors experience carbonization and aromatization processes, eventually yielding spherical carbon particles, namely submicron carbon spheres (Cheng et al. 2018).

Nicolae et al. (2020) reported that treating hydrothermal carbon solely by physical grinding does not significantly enhance its adsorption capacity or catalytic degradation performance toward organic pollutants. This is because the surface functional groups and microstructure of hydrothermal carbon materials are highly dependent on the reaction conditions, and the in situ formed carbon particles exhibit variations in size, structure, and chemical properties. In addition, different feedstocks or reaction media may lead to the formation of heterogeneous interfaces between carbon spheres, which in turn affect their electronic conductivity and surface reactivity. Saha et al. (2020) conducted HTC experiments on municipal solid waste, mixed paper fibers, after steam-autoclave pretreatment and observed comparable carbon sphere formation behavior, while Lucian et al. (2018) verified the feasibility of HTC treatment for mixed wastes, including paper, food, plastics, glass, and metals, demonstrating the broad applicability of this technology.

Cotton fibers, as a biomass feedstock, can be converted into carbon spheres during the hydrothermal carbonization process (Wei et al. 2020; Fu et al. 2020), and carbon/metal composite structures can also be generated in situ by introducing metal ions. For example, the addition of silver nitrate ($AgNO_3$) and glycerol into the reaction system promotes the reduction of Ag^+ to form silver nuclei under high-temperature hydrothermal conditions, while the carbonaceous precursors undergo heterogeneous nucleation on the silver surface to form a tightly adhered carbon layer (Niu et al. 2011). As the reaction proceeds, the silver wires gradually elongate and grow, and carbon spheres are deposited on their outer surface, eventually forming silver/carbon submicron wires with a core/shell structure (Dey et al. 2021; Liang et al. 2020). This composite architecture combines chemical stability with excellent dye adsorption performance.

In this study, cotton textile waste was employed as the carbon source to synthesize submicron carbon spheres and silver/carbon submicron wires via a hydrothermal method (Jian et al. 2023), and their

potential applications in the treatment of dye-contaminated wastewater were further investigated. Sulfuric acid was used as the catalyst, glycerol as the reducing agent, and silver nitrate as the metal precursor. The reactions were carried out at 180℃ for different durations to observe the morphological evolution of the products. To evaluate the applicability of the silver/carbon submicron wires as dye adsorbents, methylene blue (MB) was selected as a model pollutant (Wagler et al. 2022; Ikram et al. 2020), and its adsorption behavior and removal efficiency in aqueous solution were systematically examined. Through adsorption experiments and related analyses, the relationships among material structure, surface characteristics, and adsorption performance were explored (Hayat et al. 2022; Zhou et al. 2022), to assess the potential of this approach as an environmentally friendly resource valorization route (Liu et al. 2024; Zaid et al. 2020). The feasibility of applying these materials in waste fiber recycling and adsorbent fabrication was also discussed, with the aim of further expanding their practical value in environmental remediation and energy-related technologies (Liu et al. 2018; Yagub et al. 2014; Vijwani et al. 2015).

Materials and methods

Materials

The cotton fibers used in this study were supplied by the Taiwan Textile Research Institute. Sulfuric acid (H_2SO_4, 95 wt%) and methylene blue (MB) were purchased from Sigma-Aldrich. Glycerol was obtained from Island Chemical Co., and silver nitrate ($AgNO_3$) was supplied by Di-I Chemical Raw Materials Co., Ltd. The hydrothermal reactions were carried out in a 100 mL Teflon-lined stainless steel autoclave provided by Chuan-Feng Enterprise Co., Ltd.

Synthesis of submicron carbon spheres and Ag/C submicron wires

For the preparation of submicron carbon spheres, 1 g of cotton fibers were mixed with 5 wt% sulfuric acid solution and transferred into a Teflon-lined stainless steel autoclave. The hydrothermal reaction was carried out at 180℃ for 4 h. After cooling to room temperature, the resulting suspension was collected by centrifugation and repeatedly washed with deionized water until neutral pH was reached. The obtained black powders were dried and used as the submicron carbon sphere sample. For the synthesis of Ag/C submicron wires, 1 g of cotton fibers, 2.76 g of glycerol, and 0.55 g of silver nitrate were mixed with 5 wt% sulfuric acid solution to form a homogeneous precursor solution. The mixture was sealed in a Teflon-lined stainless steel autoclave and heated at 180℃ for 7 h. After the reaction, the product was separated by centrifugation and washed thoroughly with deionized water until neutral. The resulting brown powders were dried and collected as the Ag/C submicron wire sample.

Characterization techniques

The morphology and elemental composition of the submicron carbon spheres and Ag/C submicron wires were examined using scanning electron microscopy (SEM) equipped with energy-dispersive X-ray spectroscopy (EDS, Hitachi S-3400N). SEM was employed to observe the surface structure and morphological integrity of the submicron carbon spheres, while the linear architecture and distribution of the Ag/C submicron wires were analyzed to evaluate the effect of synthesis conditions on morphology control. EDS mapping and point analysis were further used to determine the elemental composition in different regions, with particular emphasis on the distribution and content of Ag in the Ag/C composite structures. The combined SEM–EDS technique enabled simultaneous investigation of microstructure and chemical composition, providing insights into the formation mechanism of submicron carbon spheres and Ag/C submicron wires and serving as a basis for subsequent functional analysis. The crystalline structure and phase composition of the samples were analyzed by X-ray diffraction (XRD) using a Bruker Enraf Nonius Kappa CCD diffractometer. The XRD patterns were used to identify the crystal structure of Ag in the Ag/C composites and to examine whether the carbon materials exhibited amorphous characteristics. Transmission electron microscopy (TEM, JEOL JEM-1400) was used to obtain high-resolution images of the samples. Selected area electron diffraction (SAED) was employed to determine the crystal structure and phase composition of the materials. Raman spectroscopy (Tokyo Instruments, Nanofinder 30) was performed to investigate the structural features of the carbon materials, with particular focus on the D band (disordered and defect-related carbon) and G band (graphitic carbon). The intensity ratio of these bands (I_D/I_G) was used to evaluate the degree of graphitization and structural defects in the carbon spheres and carbon shells. X-ray photoelectron spectroscopy (XPS, ULVAC-PHI PHI 5000 VersaProbe) was conducted to analyze the surface elemental composition and chemical bonding states of the Ag/C submicron wires. A survey scan was first performed to identify the elements present on the surface, followed by high-resolution spectra of C 1s, O 1s, Ag 3d, and S 2p to elucidate the chemical states and functional group distributions. The XPS results provide important information for understanding the surface chemistry related to adsorption behavior. Fourier-transform infrared (FT-IR) spectra were recorded using a PerkinElmer Spotlight 200i Sp2 system equipped with an AutoATR accessory. The products were mixed with KBr and pressed into pellets prior to measurement. The FT-IR spectra were used to identify surface functional groups and bonding characteristics, with particular attention to –OH, C = O, and C–O vibrational bands. The results were compared between the carbon spheres and Ag/C composites to clarify differences in functional groups. FT-IR analysis provides further insight into the adsorption mechanism of methylene blue on these materials.

Methylene blue adsorption experiments

Methylene blue (MB) adsorption experiments were conducted to evaluate the adsorption performance and kinetics of the carbon spheres and Ag/C submicron wires. The concentration of MB in aqueous solution was quantified using a UV-visible spectrophotometer (V-770, JASCO, Japan). Standard MB solutions with concentrations of 1–5 mg/L were prepared through dissolving a given amount of MB powders in deionized water, and their absorbance values were measured at the maximum absorption

wavelength (λ_{max} ≈ 662 nm). According to the Beer-Lambert law, a linear relationship exists between absorbance and concentration within this range. A calibration curve was obtained by linear regression of absorbance (A) versus MB concentration (C), which can be expressed as:

$$\mathrm{A} = \mathrm{aC} + \mathrm{b}$$

1

where A is the absorbance of MB, C is the MB concentration (mg/L), a is the slope, and b is the intercept. Because blank deionized water was used as the background, b represents the fitted intercept value and is mainly used to describe the linear correlation within the 1–5 mg/L range. The calibration equation was applied to determine the MB concentrations in adsorption samples, from which the removal efficiency and adsorption capacity were calculated. To minimize light scattering caused by suspended particles, the solutions were filtered through a membrane filter prior to UV-Vis measurement. The absorbance values obtained at different time intervals were converted into MB concentrations using the calibration equation, allowing the concentration variation with time to be evaluated and the adsorption performance of the materials to be assessed.

Results

SEM analysis of hydrothermally carbonized products

Figure 1a shows the SEM image of the product obtained from cotton fibers after hydrothermal treatment at 180℃ for 4 h. A large number of uniformly distributed carbon spheres with good sphericity can be clearly observed. The average particle size is 1.51 ± 1.38 μm, indicating that the nucleation and growth of carbon cores and spherical particles are well developed under these conditions. The corresponding EDS spectrum (Fig. 1b) reveals that carbon is the dominant element, accounting for 62.12 at%, confirming that the observed particles are indeed carbon spheres.

After extending the hydrothermal reaction time to 7 h in the presence of silver precursor, the original fibrous structure of cotton is completely transformed into Ag/C submicron wires, as shown in Fig. 1c. These structures exhibit an average diameter of 0.46 ± 0.12 μm. This morphological evolution is attributed to the progressive hydrolysis and carbonization of cellulose during the hydrothermal process, accompanied by the reduction and growth of silver species. The EDS analysis (Fig. 1d) further confirms the dual-element composition of the composite structure, with detected atomic percentages of Ag and C of 45 at% and 28 at%, respectively. The predominance of Ag indicates its leading role in the formation of the Ag/C submicron wire architecture.

XRD analysis

The XRD patterns of different samples are compared in Fig. 2. The raw cotton fibers (Fig. 2a) show only three characteristic diffraction peaks assigned to the (110), (200), and (004) planes of cellulose Iα

(JCPDS file No. 056-1719), reflecting the presence of some crystalline regions but with low crystallinity. On the other hand, the submicron carbon spheres (Fig. 2b) do not display distinct diffraction peaks, but rather exhibit only weak and broad signals, indicating that the carbon atoms are mainly arranged in a disordered manner without long-range crystalline order. In the absence of a metal-guiding effect, the hydrothermally derived carbon material is predominantly amorphous.

The Ag/C submicron wires (Fig. 2c) exhibit several strong and well-defined diffraction peaks corresponding to the (111), (200), (220), (311), and (222) planes of metallic silver, which are consistent with the standard face-centered cubic (FCC) structure (JCPDS file No. 04-0783). This indicates a high degree of crystallinity and a well-ordered lattice arrangement of the Ag cores. In general, despite Ag core is encapsulated by a carbon shell, the Ag/C submicron wires retain the high crystallinity of the FCC Ag, highlighting the critical role of silver in directing the composite structure.

TEM and SAED analysis

Figure 3a shows the TEM image of the submicron carbon spheres. The spherical structures appear uniform and dense, without obvious pores or heterogeneous phases, indicating that the spheres are mainly composed of a single carbonaceous component. This confirms the formation of compact and homogeneous carbon spheres via hydrothermal carbonization. Figure 3b presents the TEM image of the Ag/C submicron wires. A clear core/shell architecture can be observed, in which the central region with high electron density corresponds to the Ag core, while the outer region with lower electron density represents the carbon shell. The carbon layer tightly encapsulates the Ag core, forming a continuous and uniform protective coating, which indicates that carbonaceous species were effectively deposited on the surface of Ag wires during the hydrothermal process. This core/shell configuration is beneficial for enhancing the structural stability and electrical conductivity of the composite, while simultaneously providing additional surface reaction sites.

The diameter of the Ag/C submicron wires is approximately 2.01 μm with Ag core of 0.28 μm in diameter, and the carbon shell exhibits a uniform thickness without apparent cracks or delamination, further confirming the good encapsulation quality and structural integrity of the composite. Selected area electron diffraction (SAED) (Fig. 3c) patterns display several clear and continuous diffraction rings, indicating the presence of well-crystallized Ag phases. By measuring the ring radii and comparing them with JCPDS card No. 04-0783 for FCC Ag, the diffraction rings can be assigned to the (111), (200), (220), (311), and (222) planes, confirming that the metallic silver in the Ag/C submicron wires possesses a well-defined face-centered cubic (FCC) crystal structure. Because the outer carbon shell is mainly amorphous, it does not contribute regular diffraction features, and the observed SAED rings attribute predominantly to the Ag core. The consistency between SAED and XRD results further verifies the crystalline structure and stability of the Ag phase in the hydrothermally synthesized Ag/C submicron wires.

Raman spectroscopy analysis

The Raman spectra of the submicron carbon spheres (Fig. 4a) and Ag/C submicron wires (Fig. 4b) were compared to evaluate their structural differences. Both materials exhibit characteristic Raman peaks of carbon-based materials. The G-band appears at 1559 $cm^{-1}$for the submicron carbon spheres and 1580 $cm^{-1}$for the Ag/C submicron wires, corresponding to the sp^2-hybridized carbon in graphitic domains, indicating the presence of graphitized structures in both samples. The D-band, associated with defects and disordered carbon, appears at 1347 cm^{-1} for the carbon spheres and 1354 cm^{-1} for the Ag/C wires, corresponding to sp^3-hybridized carbon induced by structural defects. The intensity ratio of these bands (I_D/I_G) was further analyzed, showing a value of 0.85 for Ag/C submicron wires, slightly lower than 0.87 for the carbon spheres. A lower I_D/I_G ratio indicates a higher degree of graphitization; therefore, the Ag/C submicron wires possess a more ordered carbon shell structure compared to the purely carbonaceous spheres. This enhanced graphitization is attributed to the directing effect of silver during the hydrothermal carbonization process, which facilitates the ordering of the carbon framework and reduces structural defects. In contrast, carbon spheres derived solely from cellulose lack metallic guidance, resulting in slightly lower graphitization and higher structural disorder. These results not only reveal differences in structural characteristics between the two materials but also highlight the crucial role of silver in improving the order and stability of carbon-based composites.

XPS surface elemental analysis

X-ray photoelectron spectroscopy (XPS) was employed to investigate the surface elemental composition and chemical states of the Ag/C submicron wires. As shown in the survey spectrum (Fig. 5a), characteristic peaks of C 1s, O 1s, Ag 3d, and S 2p are clearly observed, along with an O KLL Auger peak at approximately 980–1000 eV. This confirms that the material is primarily composed of carbon, oxygen, silver, and a small amount of sulfur, indicating successful loading of Ag onto the carbon-based surface. Ag 3d spectrum (Fig. 5b) shows two symmetric peaks at 367.5 eV and 373.5 eV, corresponding to Ag $3d_{5/2}$ and Ag $3d_{3/2}$, respectively, with a spin–orbit splitting of ~ 6.0 eV, characteristic of metallic silver (Ag^0). This suggests that silver exists predominantly in its zero-valent state without significant oxidation, which is beneficial for electron transport and surface reactivity. The C 1s spectrum (Fig. 5c) was deconvoluted into four components: 284.8 eV corresponding to C-C/C□H bonds, forming the primary carbon backbone; 286.1 eV assigned to C□O bonds; 286.8 eV to C = O; and 288.5 eV to O□C = O, indicating the presence of hydroxyl, ether, and carboxyl functional groups on the carbon surface. These oxygen-containing groups can act as active adsorption sites. The O 1s spectrum (Fig. 5d) was fitted with three components at 529.9 eV assigned as lattice oxygen or metal–oxygen bonds, 531.3 eV assigned as hydroxyl or defect oxygen, and 532.5 eV assigned as adsorbed oxygen or carboxyl oxygen, demonstrating the surface richness in oxygen functionalities, which improves hydrophilicity and surface reactivity. Excluding the contribution of residual SO_4^{2-}, the binding energy of O 1s assigned to organic sulfur species are 532.5 eV. The S 2p spectrum (Fig. 5e) displays a spin–orbit doublet at 167.9 eV and 169.1 eV, corresponding to S $2p_{3/2}$ and S $2p_{1/2}$, suggesting that sulfur exists primarily in oxidized forms. Although present in minor amounts, these sulfur-containing groups may influence surface charge distribution, thereby promoting adsorption of cationic dye molecules. Excluding the contribution of

residual SO_4^{2-}, the binding energy of S 2p assigned to organic sulfur species are 167.9 eV, respectively. The noticeable residuals in the S 2p fitting, particularly in the 168.5–169.5 eV range, are primarily attributed to the low signal-to-noise ratio due to the low sulfur concentration of 0.78 at%. Additionally, the mismatch may suggest a distribution of different oxidation states or chemical environments (e.g., various sulfonate and sulfone species) rather than a single ideal doublet, which is common for hydrothermally functionalized carbon materials. The XPS results show that the Ag/C submicron wires possess a surface rich in oxygen- and sulfur-containing functional groups, along with well-dispersed metallic silver nanoparticles. The synergistic effect of surface functional groups and Ag nanoparticles provides multiple active sites, which may play a critical role in dye adsorption.

FT-IR analysis

The functional groups of the submicron carbon spheres and Ag/C submicron wires were investigated using Fourier-transform infrared spectroscopy (FT-IR), as shown in Fig. 6. For the submicron carbon spheres (Fig. 6a), a broad absorption band at 3423 cm^{-1} corresponds to the stretching vibrations of -OH groups, indicating that hydroxyl groups or adsorbed water molecules are still present on the carbon surface. Peaks at 2928 $cm^{-1}$and 2856 $cm^{-1}$are attributed to the asymmetric and symmetric stretching vibrations of aliphatic $-CH_2-$ groups, reflecting residual organic chain segments in the carbon matrix. The absorption near 1703 cm^{-1} is assigned to C = O stretching, while the band at 1622 cm^{-1} corresponds to conjugated C = C or aromatic ring vibrations. Additional peaks at 1465 cm^{-1} and 1381 $cm^{-1}$are attributed to $-CH_2-$ bending and $-CH_3$ deformation vibrations, respectively (Zhang et al. 2022; Gao et al. 2016). FT-IR spectrum of Ag/C submicron wires (Fig. 6b) exhibits a –OH related band at 3345 cm^{-1}, with slightly altered intensity and red shift compared to the carbon spheres, suggesting that the presence of Ag may affect the distribution of surface hydroxyl groups. The $-CH_2-$stretching vibrations at 2923 cm^{-1} and 2852 cm^{-1} remain, indicating the preservation of the carbon backbone. Notably, new absorption bands appear at 1688 cm^{-1} and 1581 cm^{-1}, assigned to C = O and aromatic C = C vibrations, respectively, implying potential coordination or electronic interactions between Ag and carbon surface functional groups. The peaks at 1449 cm^{-1} and 1380 cm^{-1} also indicate the continued presence of hydrocarbon structures, although their intensities and positions are slightly red shifted due to the altered chemical environment after Ag incorporation (Niu et al. 2011; Zhang et al. 2022). These results demonstrate that the Ag/C submicron wires retain the original functional groups of the carbon material, while the introduction of Ag modifies the surface electronic distribution and vibrational characteristics of the functional groups. This interfacial interaction between Ag and carbon is expected to enhance the activity of the material in adsorption and surface reaction applications.

Methylene blue adsorption

Methylene blue adsorption experiments were carried out to evaluate the adsorption performance of the carbon spheres and Ag/C submicron wires as well as the adsorption mechanisms. To quantify the adsorption behavior of MB, a UV-Vis calibration curve was first established. As shown in Fig. 7a, MB solutions in the 1–5 mg/L concentration range exhibited a strong linear relationship between

absorbance and concentration, with the linear regression equation expressed as $y = 0.23874x + 0.001656$ and a corresponding coefficient of determination $R^2 = 0.99906$. This result confirms the accuracy and reproducibility of the UV-Vis measurement method, enabling reliable quantification of MB concentration during subsequent adsorption experiments. Adsorption experiments were conducted using an initial MB concentration of 5 mg/L, which falls within the linear range of the calibration curve. Figure 7b compares the adsorption behavior of submicron carbon spheres and Ag/C submicron wires at different contact times. During the initial 5 min, a rapid decrease in MB concentration was observed, indicating efficient adsorption within a short contact time. Notably, the concentration of MB decreased more sharply within the first 5 minutes for Ag/C submicron wires compared to carbon spheres, demonstrating that the introduction of Ag enhances adsorption kinetics. This rapid adsorption is attributed to the high density of available active sites on the Ag/C submicron wire surface, facilitating effective adsorption and binding of MB molecules. The strong interfacial interaction between silver and the carbon shell, which is evidenced through the red shift of IR peaks on Ag/C submicron wires, is expected to modulate the electronic structure of the carbon surface, thereby enhancing the density and activity of adsorption sites for cationic dye molecules. Furthermore, Ag incorporation likely modifies the surface polarity and interfacial properties of the carbon material, enhancing the interaction between MB molecules and the adsorbent surface. Since MB is a cationic dye (MB^+), its adsorption onto Ag/C submicron wires is governed by multiple interfacial mechanisms. First, FT-IR analysis (Fig. 6) indicates the presence of -OH and C=O functional groups on the Ag/C surface. These groups can deprotonate in aqueous solution, forming negatively charged $-O^-$ or $-COO^-$ active sites that strongly attract MB^+ via electrostatic interactions, serving as a primary driving force for adsorption. Second, the retained aromatic carbon structures in Ag/C submicron wires enable π-π stacking interactions with the aromatic rings of MB molecules, further stabilizing their adsorption. Additionally, Ag incorporation can modulate the electronic structure and local charge distribution of the carbon surface, potentially promoting coordination interactions and electron transfer effects between MB molecules and surface active sites, thereby strengthening interfacial binding. In contrast, submicron carbon spheres possess fewer surface negative charges and lower electronic activity, resulting in reduced contribution from electrostatic and chemical adsorption toward MB^+. Combining FT-IR analysis (Fig. 6) with adsorption results (Fig. 7), it is evident that Ag incorporation not only modifies the distribution of surface functional groups and electronic structure but also significantly enhances the adsorption efficiency and capacity for MB. The adsorption rate gradually slows after approximately 10–25 min, indicating that most surface active sites become occupied and the system approaches equilibrium.

Discussion

Synthesis mechanism of submicron carbon spheres

Figure 8 illustrates the proposed formation mechanism of submicron carbon spheres. Cotton fibers are primarily composed of cellulose, a high-molecular-weight polysaccharide consisting of repeating β-1,4-linked disaccharide units. Under hydrothermal conditions in the presence of sulfuric acid (H_2SO_4), the

acidic environment catalyzes the hydrolysis of cellulose chains, progressively breaking them down into soluble oligosaccharides and glucose monomers. This acid-catalyzed hydrolysis disrupts the crystalline structure of cellulose, releasing reactive glucose molecules into the solution. With increasing reaction temperature, the liberated glucose undergoes dehydration to form 5-hydroxymethylfurfural (HMF), a key intermediate containing highly reactive carbonyl and hydroxymethyl functional groups. Under acidic conditions, HMF molecules readily undergo condensation and polymerization reactions, generating carbon-rich polymeric precursors. As the hydrothermal reaction progresses, these carbonaceous precursors aggregate and undergo aromatization, transforming the internal structure from oxygenated organic compounds to an amorphous aromatic carbon framework. The concentration of carbon precursors and the reaction temperature critically influence the resulting morphology. Once the concentration reaches a critical threshold, homogeneous nucleation occurs, forming initial carbon nuclei. These nuclei subsequently grow through diffusion and self-assembly processes, ultimately yielding spherical carbon structures. The formation of the spherical morphology is driven by the minimization of interfacial energy, allowing the carbon spheres to adopt a thermodynamically stable shape during growth. Upon prolonged hydrothermal treatment and subsequent carbonization, the carbon precursors further lose oxygen and hydrogen, resulting in highly stable carbon spheres. The final products exhibit uniform dispersion, submicron-scale particle size, and surface functional groups such as hydroxyl and carboxyl moieties, which are beneficial for subsequent surface modification or metal loading. In summary, the transformation pathway can be described as: cellulose → glucose → HMF → carbonaceous precursors → carbon spheres. This mechanism not only clarifies the chemical conversion of cotton fibers under acid-assisted hydrothermal conditions but also demonstrates the feasibility of deriving functional carbon materials from natural polysaccharides, providing a promising route for high-value utilization of biomass waste.

Synthesis mechanism of Ag/C submicron wires

Figure 9 illustrates the proposed formation mechanism of Ag/C submicron wires derived from cotton fibers under acid-assisted hydrothermal conditions. In the initial stage, Ag^{+} ions are gradually reduced to metallic silver by glycerol, and the resulting silver atoms self-assemble into one-dimensional nanowires. Subsequently, cellulose undergoes acid-catalyzed hydrolysis to generate glucose, which is further dehydrated under hydrothermal conditions to form 5-hydroxymethylfurfural (HMF) containing reactive functional groups that condense and polymerize into carbonaceous precursors. These carbonaceous precursors then nucleate heterogeneously on the silver nanowires, forming carbon spheres that progressively coat the silver cores. As the reaction proceeds, the carbon spheres on the silver cores gradually interconnect to develop a continuous carbon shell. Finally, this process yields Ag/C submicron wires with a well-defined core-shell architecture, emphasizing the synergistic coupling between metal reduction and carbonization, where silver nanowires act as nucleation templates guiding the oriented growth of the carbon shell.

Adsorption kinetics

The adsorption behavior of MB onto the submicron carbon spheres and Ag/C submicron wires was first evaluated using the pseudo-first-order kinetic model, expressed in its linear form as:

$$\ln(q_e - q_t) = \ln q_e - k_1 t$$

2

where q_e (mg g^{-1}) is the equilibrium adsorption capacity, q_t (mg g^{-1}) is the adsorption capacity at time t, and k_1(min^{-1}) is the pseudo-first-order rate constant. As shown in Fig. 10a, both carbon spheres and Ag/C submicron wires exhibited partial linearity under this model during the initial adsorption stage. However, a significant deviation from linearity was observed at longer contact times, particularly for the Ag/C submicron wires. The calculated equilibrium adsorption capacities ($q_{e,cal}$) obtained from the pseudo-first-order model (Table 1) were substantially lower than the experimentally determined values ($q_{e,exp}$), with correlation coefficients (R^2) of 0.822 and 0.718 for carbon spheres and Ag/C wires, respectively, indicating that the pseudo-first-order model inadequately describes the adsorption process.

Table 1
Kinetic parameters for MB adsorption on submicron carbon spheres and Ag/C submicron wires calculated using pseudo-first-order (PFO) and pseudo-second-order (PSO) models

Adsorbent	$q_{e,exp}$ **(mg/g)**	**Model**	$q_{e,cal}$ **(mg/g)**	**k (min^{-1} or g/mg·min)**	R^2
Carbon spheres	3.354	PFO	0.827	0.106	0.822
		PSO	3.499	0.213	0.998
Ag/C submicron wires	4.518	PFO	1.298	0.1748	0.718
		PSO	4.662	0.247	0.999

Subsequently, the pseudo-second-order kinetic model was applied to further elucidate the adsorption mechanism, described by:

$$\frac{t}{q_t} = \frac{1}{k_2 q_e^2} + \frac{t}{q_e}$$

3

where k_2 (g mg^{-1} min^{-1}) is the pseudo-second-order rate constant. As illustrated in Fig. 10b, the linear plots of t/q_t versus t exhibited excellent correlation for both adsorbents, confirming that the pseudo-second-order model more accurately represents the adsorption kinetics. This observation suggests that the adsorption rate is predominantly controlled by chemisorption involving surface active sites rather than diffusion-limited physical adsorption.

Notably, the Ag/C submicron wires displayed a higher adsorption capacity and faster kinetic rate compared to carbon spheres. The calculated $q_{e,cal}$values were 3.499 mg g^{-1} and 4.662 mg g^{-1} for carbon spheres and Ag/C wires (Table 1), respectively, closely matching the experimental values of 3.354 mg g^{-1} and 4.518 mg g^{-1}, with correlation coefficients approaching unity ($R^2 = 0.998$ and 0.999). Additionally, the pseudo-second-order rate constant for Ag/C wires ($k_2 = 0.247$ g $mg^{-1}min^{-1}$) was higher than that for carbon spheres ($k_2 = 0.213$ g $mg^{-1}min^{-1}$), indicating that the presence of Ag enhances the adsorption rate. The pseudo-second-order model provided an excellent fit to the adsorption data, highlighting that the MB adsorption on both carbon spheres and Ag/C submicron wires is predominantly chemisorption-controlled, with Ag incorporation significantly enhancing the adsorption kinetics and capacity. The improved performance can be attributed to the increased number of surface active sites, enhancing interactions with dye molecules. In summary, these findings provide structural and chemical insight into the methylene blue adsorption performance, confirming that the synergy between Ag nanoparticles and the carbon framework is the key to superior removal efficiency.

Conclusions

In this study, submicron carbon spheres and Ag/C submicron wires were prepared from waste cotton fibers via an acid-assisted hydrothermal process, and their structure–property–adsorption relationships were clarified. SEM-EDS results confirmed the complete conversion of cotton fibers into carbon spheres (1.51 ± 1.38 μm, 62.12 at% C) at 180 ℃ for 4 h, and into Ag/C submicron wires (0.46 ± 0.12 μm, 45 at% Ag, 28 at% C) at 180 ℃ for 7 h, revealing the key role of reaction conditions in morphology control. Structural characterizations (XRD, TEM, SAED, Raman) demonstrated that the Ag/C submicron wires possess a well-defined core–shell architecture with highly crystalline FCC Ag cores and a more graphitized, ordered carbon shell compared with pure carbon spheres. Surface analyses (XPS, FT-IR) showed that Ag/C submicron wires are enriched with oxygen- and sulfur-containing functional groups and metallic silver, providing multiple active sites and enhanced surface reactivity. Methylene blue adsorption tests further revealed that Ag/C submicron wires exhibit faster adsorption kinetics and superior removal performance than carbon spheres, attributable to the synergistic effect between the silver core and the functionalized carbon shell. These findings highlight a simple and sustainable route to upcycle cotton textile waste into functional Ag/C carbon materials with promising potential for dye removal and environmental remediation.

Declarations

Acknowledgments The authors would like to acknowledge the financial support for this research by National Science and Technology Council, Taiwan, under Grant No. NSTC 114-2622-E-019-001 and No. 114-2813-C-034-006-E.

Author contribution Hung-Bin Lee: Writing – review & editing, Writing – original draft, Methodology, Investigation, Project administration. Yu-Wei Tseng: Writing – original draft, Investigation, Formal

analysis. Ming-Yuan Lin: Writing – review & editing, Visualization, Validation. Ming-Chih Kuo: Writing – review & editing, Writing – original draft, Methodology, Investigation, Supervision.

Funding This work was supported by National Science and Technology Council, Taiwan, under Grant No. NSTC 114-2622-E-019-001 and No. 114-2813-C-034-006-E.

Data availability Data are available upon reasonable request.

Ethical approval This is not applicable.

Consent to participate This is not applicable.

Consent for publication This is not applicable.

Competing interests The authors declare no competing interests.

References

1. Acharya S, Hu Y, Abidi N (2021) Cellulose dissolution in ionic liquid under mild conditions: Effect of hydrolysis and temperature. Fibers 9:1–14. https://doi.org/10.3390/fib9010005
2. Ahn J, Pealer C, Kim S (2024) Analysis of carbon dots synthesized at different hydrothermal carbonization temperatures and their ferric ion detection performances. Phys Status Solidi B 261:2300345. https://doi.org/10.1002/pssb.202300345
3. Anžlovar A, Žagar E (2022) Cellulose structures as a support or template for inorganic nanostructures and their assemblies. Nanomaterials 12:1837. https://doi.org/10.3390/nano12111837
4. Basso D (2016) Agro-industrial waste to solid biofuel through hydrothermal carbonization. Waste Manag 47:114–121. https://doi.org/10.1016/j.wasman.2015.05.013
5. Cao Y, He M, Dutta S, Luo G, Zhang S, Tsang DCW (2021) Hydrothermal carbonization and liquefaction for sustainable production of hydrochar and aromatics. Renew Sustainable Energy Rev 152:111722. https://doi.org/10.1016/j.rser.2021.111722
6. Cheng F, Li X (2018) Preparation and application of biochar-based catalysts for biofuel production. Catalysts 8:346. https://doi.org/10.3390/catal8090346
7. Dey S, Chakraborty P, Rana DK, Pramanik S, Basu S (2021) Surfactant-free synthesis of carbon-supported silver (Ag/C) nanobars as an efficient electrocatalyst for alcohol tolerance and oxidation of sodium borohydride in alkaline medium. SN Appl Sci 3:1–12. https://doi.org/10.1007/s42452-021-04601-9
8. Fu F, Yang D, Zhang W, Wang H, Qiu X (2020) Green self-assembly synthesis of porous lignin-derived carbon quasi-nanosheets for high-performance supercapacitors. Chem Eng J 392:123721. https://doi.org/10.1016/j.cej.2019.123721

9. Gao P, Zhou Y, Meng F, Zhang Y, Liu Z, Zhang W, Xue G (2016) Preparation and characterization of hydrochar from waste eucalyptus bark by hydrothermal carbonization. Energy 97:238–245. https://doi.org/10.1016/j.energy.2015.12.123
10. Hayat M, Shah A, Nisar J, Shah I, Haleem A, Ashiq MN (2022) A novel electrochemical sensing platform for the sensitive detection and degradation monitoring of methylene blue. Catalysts 12:306. https://doi.org/10.3390/catal12030306
11. Ikram M, Raza A, Imran M, Hamid AU, Shahbaz A, Ali S (2020) Hydrothermal synthesis of silver decorated reduced graphene oxide (rGO) nanoflakes with effective photocatalytic activity for wastewater treatment. Nanoscale Res Lett 15:95. https://doi.org/10.1186/s11671-020-03323-y
12. Jian X, Wang Y, Zhu R, Pan Y, Ye H, Zeng X (2023) One-pot biosynthesis of carbon-coated silver nanoparticles using palm leaves as a reductant and a carbon source. ACS Omega 8:23820–23828. https://doi.org/10.1021/acsomega.3c01554
13. Kalabek NA, Babaarslan O (2016) Fiber Selection for the Production of Nonwovens. In: Non-woven Fabrics, IntechOpen. https://doi.org/10.5772/61977
14. Liang M, Liu X, Wang L, He Y, Huang F, Li B, Zhang K, Tian H (2020) Preparation and characterization of nano silver immobilized hydrochar derived from hydrothermal carbonization of tobacco stem. Mater Res Express 7:015611. https://doi.org/10.1088/2053-1591/ab6764
15. Liu J, Jiang P, Tian S, Ren M, Ren H, Yang H (2024) Preparation and characterization of silver-carbon composite semitransparent hollow microspheres for surface-enhanced Raman scattering. Chin J Anal Chem 52:100361. https://doi.org/10.1016/j.cjac.2024.100374
16. Liu X, Yang R, Xu M, Ma C, Li W, Yin Y, Huang Q, Wu Y, Li J, Liu S (2018) Hydrothermal synthesis of cellulose nanocrystal-grafted-acrylic acid aerogels with superabsorbent properties. Polymers 10:1168. https://doi.org/10.3390/polym10101168
17. Lucian M, Volpe M, Gao L, Piro G, Goldfarb JL, Fiori L (2018) Impact of hydrothermal carbonization conditions on the formation of hydrochars and secondary chars from the organic fraction of municipal solid waste. Fuel 233:257–268. https://doi.org/10.1016/j.fuel.2018.06.060
18. Muhlack RA, Potumarthi R, Jeffery DW (2018) Sustainable wineries through waste valorisation: A review of grape marc utilisation for value-added products. Waste Manag 72:99–118. https://doi.org/10.1016/j.wasman.2017.11.011
19. Nicolae SA, Au H, Modugno P, Luo H, Szego AE, Qiao M, Li L, Yin W, Heeres HJ, Berged N, Titirici MM (2020) Recent advances in hydrothermal carbonisation: from tailored carbon materials and biochemicals to applications and bioenergy. Green Chem 22:4747–4800. https://doi.org/10.1039/D0GC00998A
20. Niu H, Wu X, Qiu M, Gao Y, Song C, Mao C, Zhang S, Liu H, Wu J (2011) A study on surfactant-free growth of silver-carbon nanocables by H2SO4-mediated hydrothermal process. J Mater Res 26:2780–2794. https://doi.org/10.1557/jmr.2011.251
21. Paksung N, Pfersich J, Arauzo PJ, Jung D, Kruse A (2020) Structural effects of cellulose on hydrolysis and carbonization behavior during hydrothermal treatment. ACS Omega 5:12210–12223.

https://doi.org/10.1021/acsomega.0c00737

22. Peng J, Kang X, Zhao S, Zhao P, Ragauskas AJ, Si C, Xu T, Song X (2023) Growth mechanism of glucose-based hydrochar under the effects of acid and temperature regulation. J Colloid Interface Sci 630:654–665. https://doi.org/10.1016/j.jcis.2022.10.044
23. Qi Y, Zhang M, Qi L (2016) Mechanism for the formation and growth of carbonaceous spheres from sucrose by hydrothermal carbonization. RSC Adv 6:20814–20823. https://doi.org/10.1039/C5RA26725K
24. Saha N, McGaughy K, Reza MT (2020) Elucidating hydrochar morphology and oxygen functionality change with hydrothermal treatment temperature ranging from subcritical to supercritical conditions. J Anal Appl Pyrol 152:104965. https://doi.org/10.1016/j.jaap.2020.104965
25. Sharma R, Jasrotia K, Singh N, Ghosh P, Srivastava S, Sharma NR, Singh J, Kanwar R, Kumar A (2020) A comprehensive review on hydrothermal carbonization of biomass and its applications. Chem Afr 3:1–19. https://doi.org/10.1007/s42250-019-00098-3
26. Vijwani H, Nadagouda MN, Namboodiri V, Mukhopadhyay SM (2015) Hierarchical hybrid carbon nano-structures as robust and reusable adsorbents: Kinetic studies with model dye compound. Chem Eng J 268:197–207. https://doi.org/10.1016/j.cej.2015.01.027
27. Wagler P, Scheible J, Habekost A (2022) Methylene blue - New chemistry experiments for university education. World J Chem Educ 10:137–148. https://doi.org/10.12691/wjce-10-4-3
28. Wei J, Liao M, Ma A, Chen Y, Duan Z, Hou X, Li M, Jiang N, Yu J (2020) Enhanced thermal conductivity of polydimethylsiloxane composites with carbon fiber. Compos Commun 17:141–146. https://doi.org/10.1016/j.coco.2019.12.004
29. Yagub MT, Sen TK, Afroze S (2014) Dye and its removal from aqueous solution by adsorption: A review. Adv Colloid Interface Sci 209:172–184. https://doi.org/10.1016/J.CIS.2014.04.002
30. Zaid MHM, Abdullah J, Yusof NA, Wasoh H, Sulaiman Y, Noh MFM, Issa R (2020) Reduced graphene oxide/TEMPO-nanocellulose nanohybrid-based electrochemical biosensor for the determination of Mycobacterium tuberculosis. J Sens 2020:11. https://doi.org/10.1155/2020/4051474
31. Zhang L, Wang Q, Xu F, Wang Z, Zhang G (2022) Insights into the evolution of chemical structures in hydrochars from hydrothermal carbonization of PVC. J Energy Inst 105:323–333. https://doi.org/10.1016/j.joei.2022.09.004
32. Zhou F, Li K, Hang F, Zhang Z, Chen P, Weia L, Xie C (2022) Efficient removal of methylene blue by activated hydrochar prepared by hydrothermal carbonization and NaOH activation of sugarcane bagasse and phosphoric acid. RSC Adv 12:1885–1896. https://doi.org/10.1039/D1RA08325B

Figures

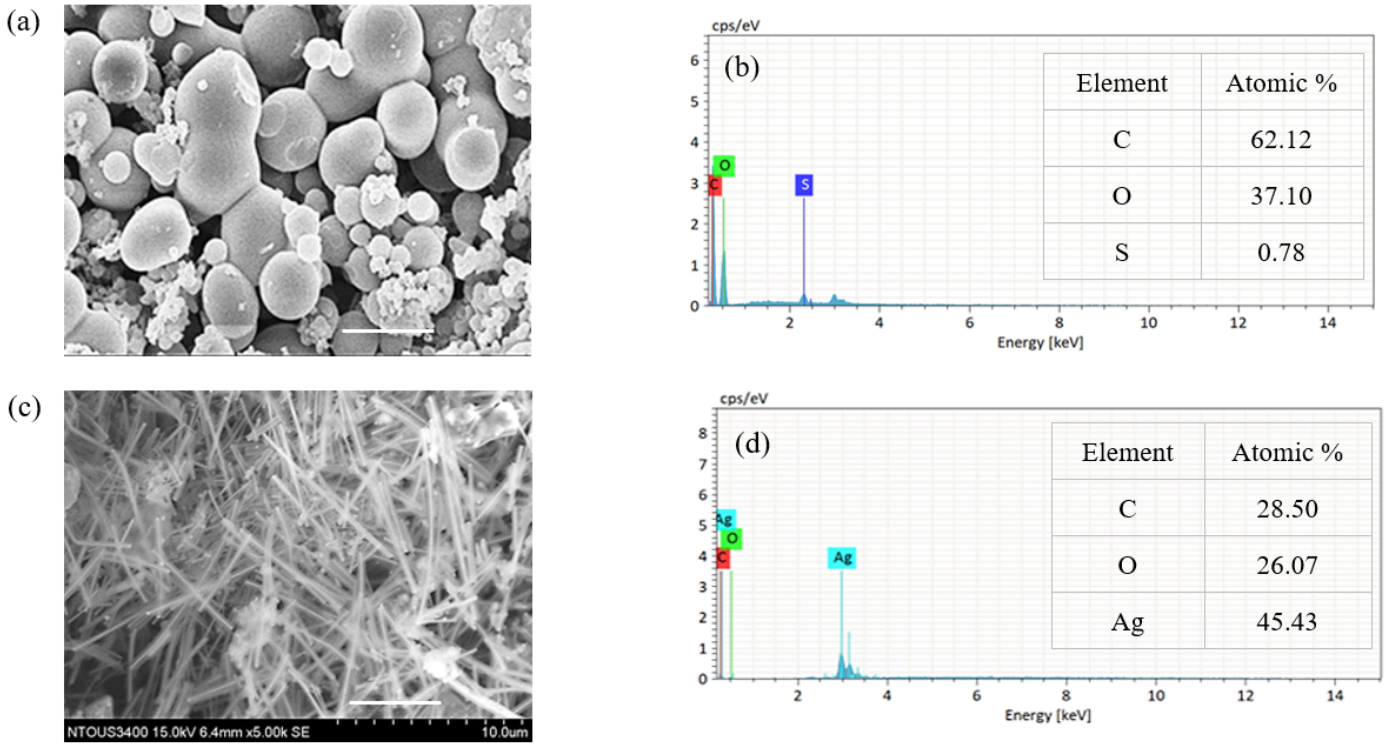


Figure 1

(a) SEM image of submicron carbon spheres synthesized from cotton fibers by hydrothermal treatment at 180°C for 4 h, **(b)** EDS spectrum and elemental composition of the sample of the submicron carbon spheres, **(c)** SEM image of Ag/C submicron wires obtained after hydrothermal treatment at 180°C for 7 h in the presence of $AgNO_3$ and glycerol, **(d)** EDS spectrum and elemental composition of the sample of the Ag/C submicron wires

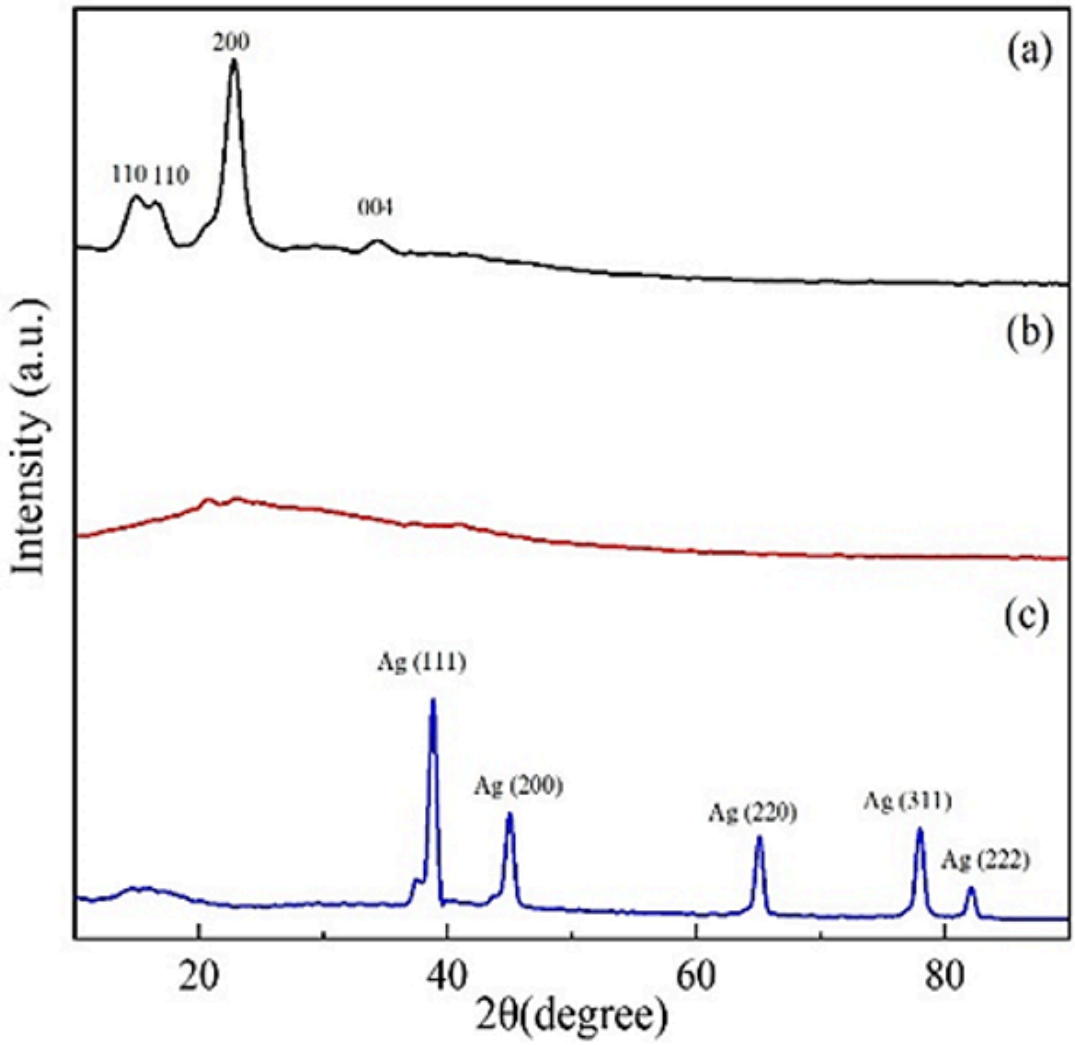


Figure 2

XRD patterns of **(a)** pristine cotton fibers, **(b)** submicron carbon spheres, and **(c)** Ag/C submicron wires

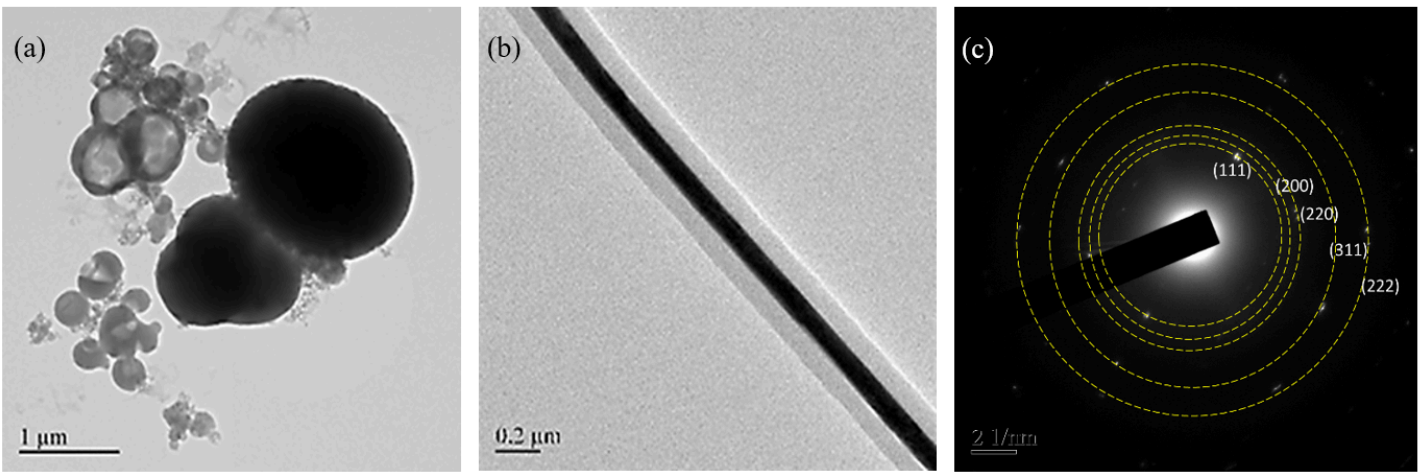


Figure 3

(a) TEM image of submicron carbon spheres, **(b)** TEM image of Ag/C submicron wires, and **(c)** SAED image of Ag/C submicron wires

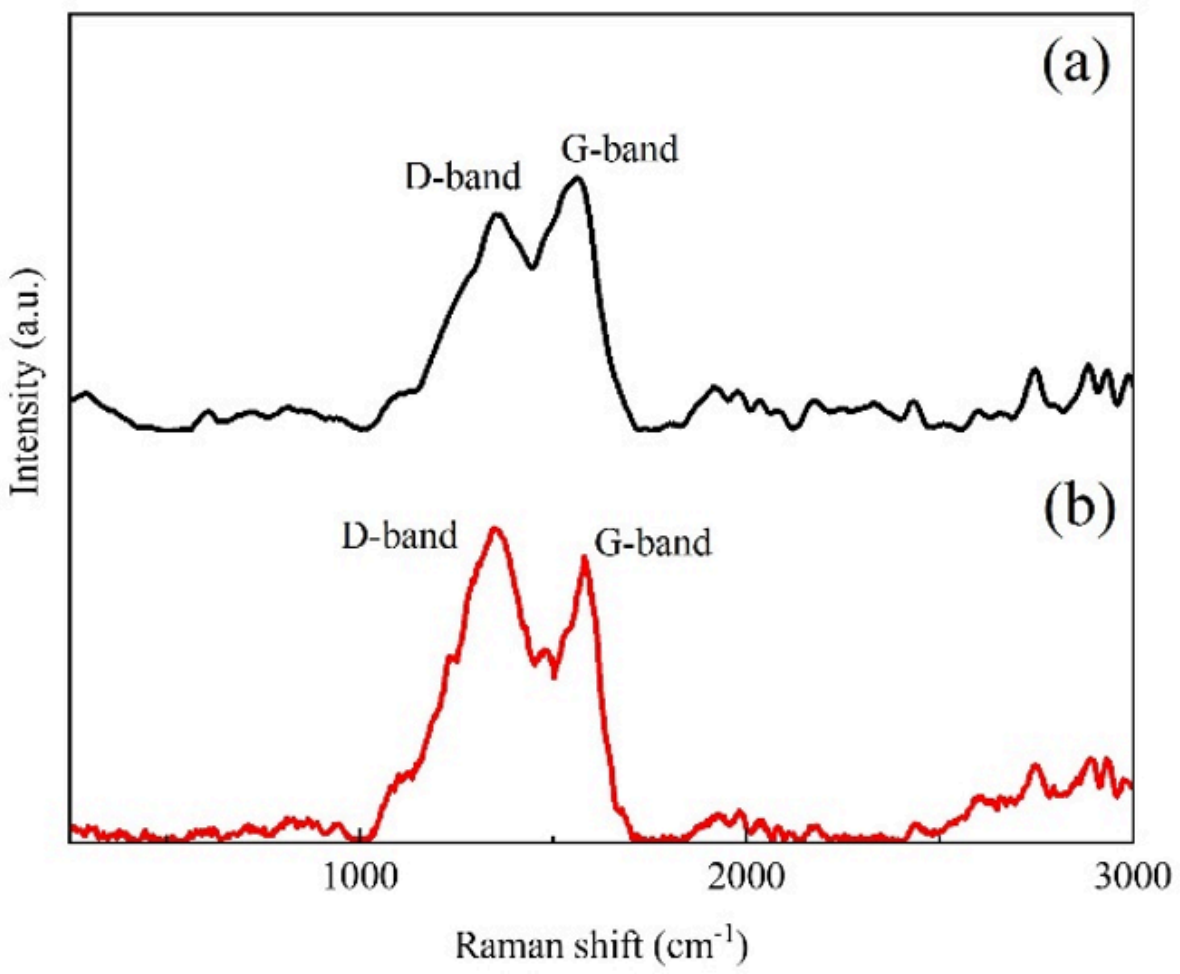


Figure 4

Raman spectra of **(a)**submicron carbon spheres and **(b)**Ag/C submicron wires, showing the D and G bands and their relative intensity differences

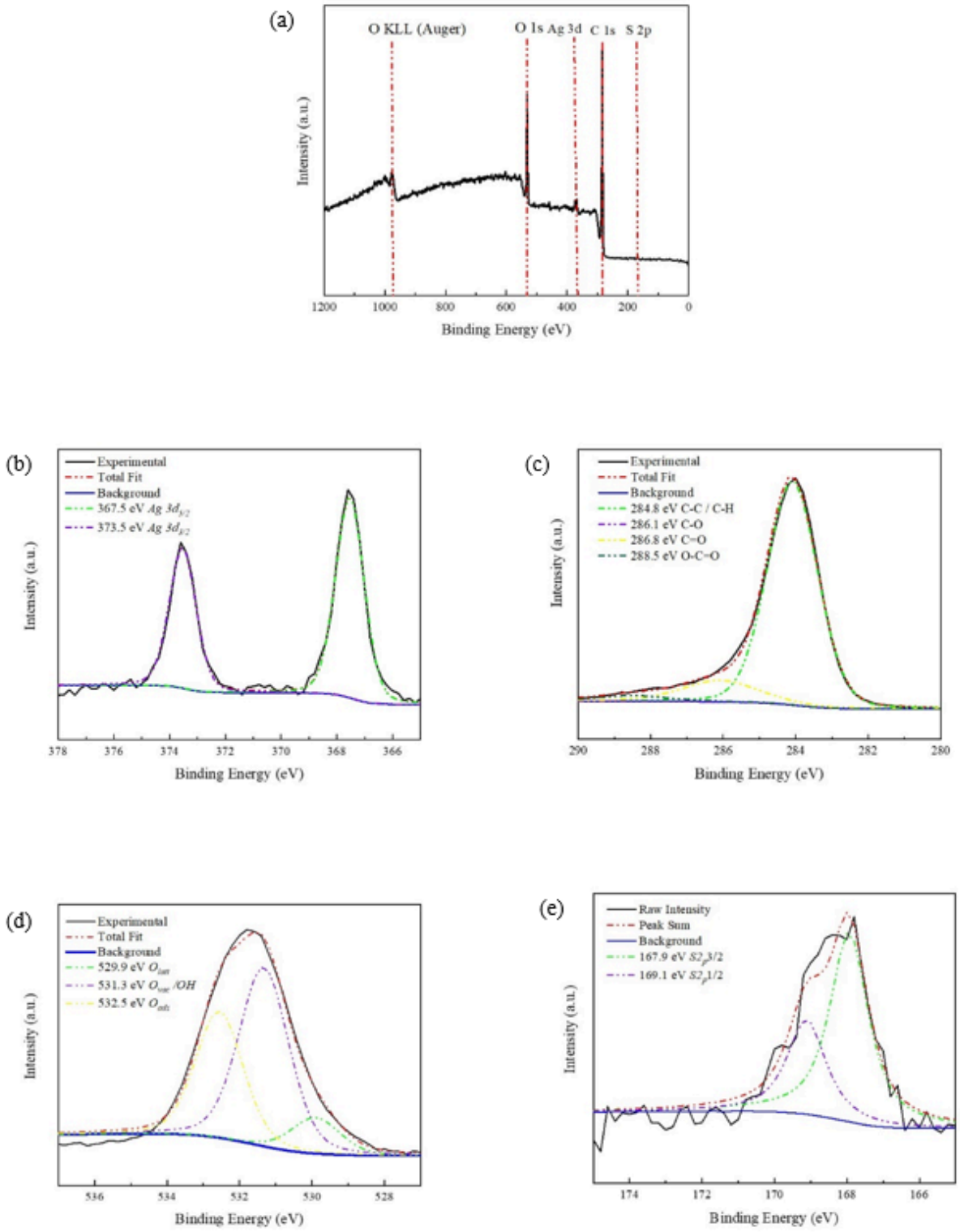


Figure 5

XPS analysis of Ag/C submicron wires: **(a)**survey spectrum, **(b)** Ag 3d spectrum, **(c)** C 1s spectrum, **(d)** O 1s spectrum, and **(e)** S 2p spectrum

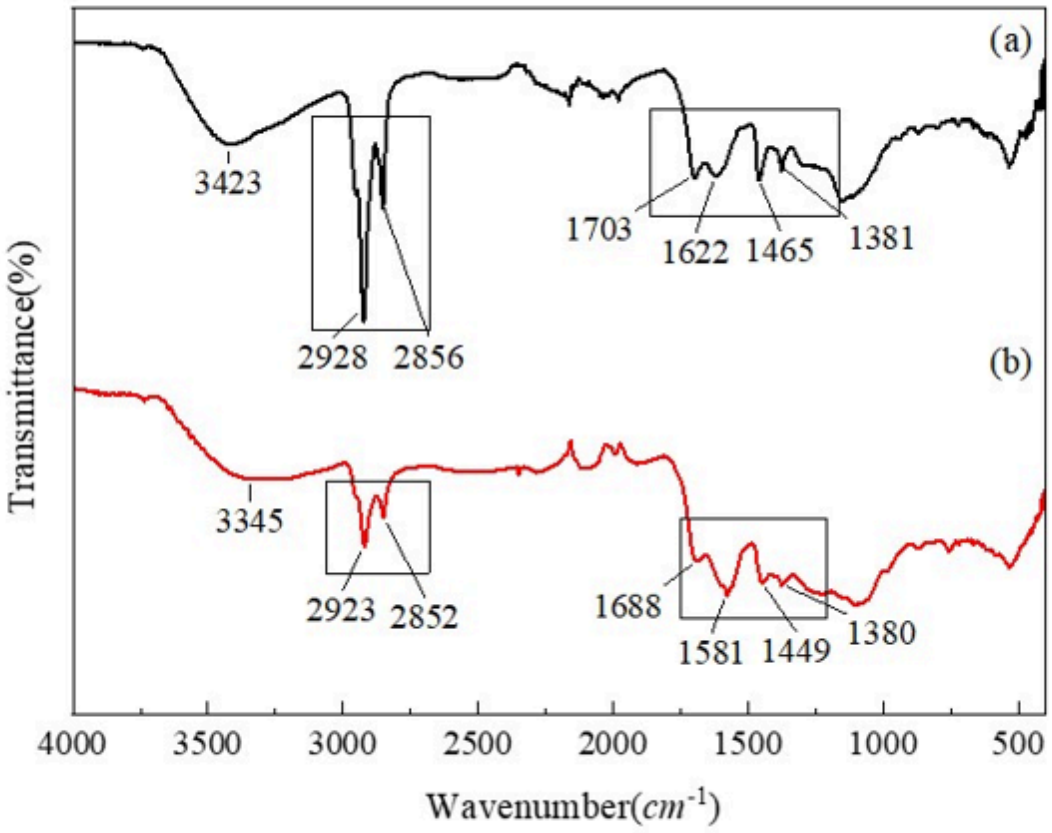


Figure 6

FT-IR spectra of **(a)** submicron carbon spheres and **(b)** Ag/C submicron wires

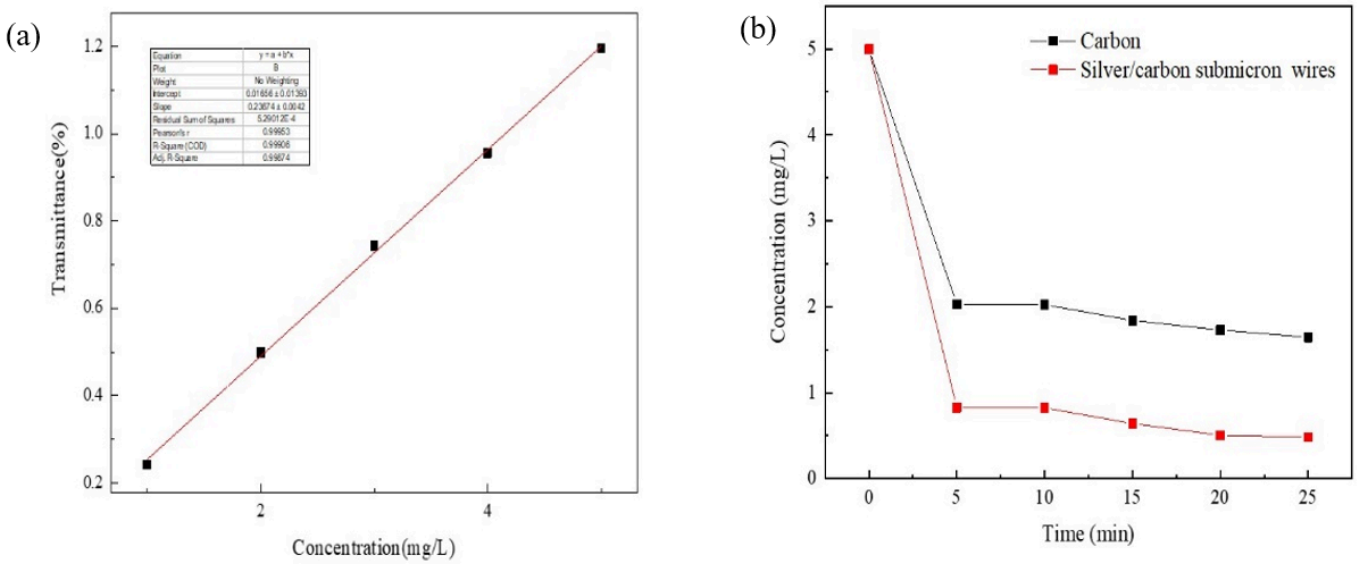


Figure 7

(a) Calibration curve of methylene blue (MB) in the concentration range of 1-5 mg/L, **(b)**MB adsorption by submicron carbon spheres and Ag/C submicron wires within the initial 25 min

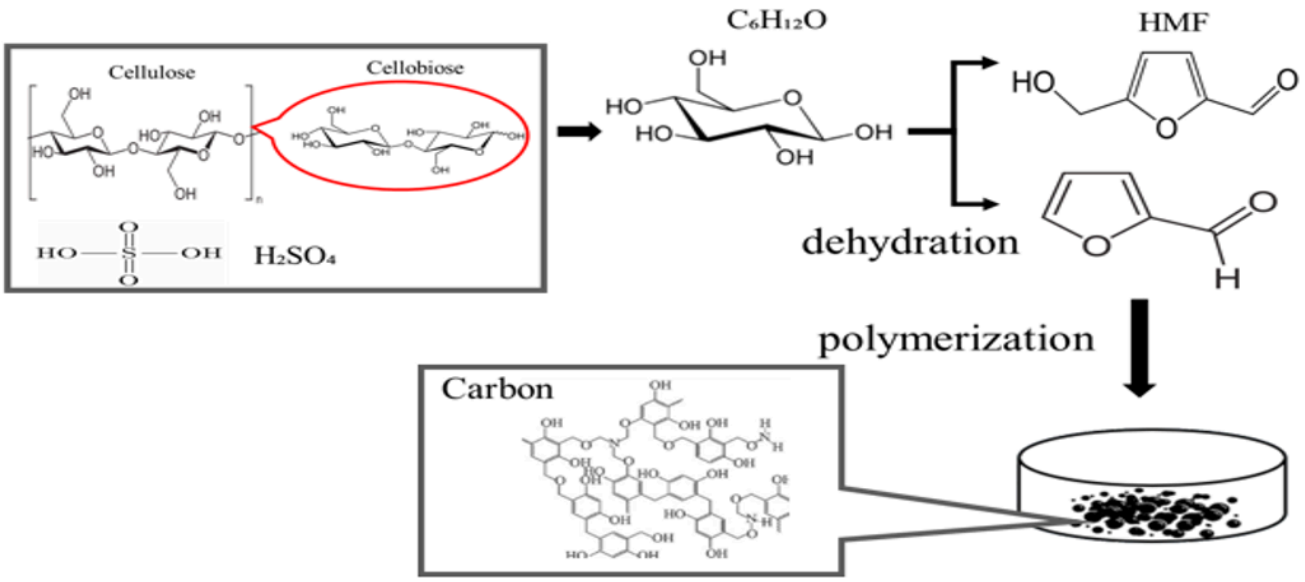


Figure 8

Schematic illustration of the formation mechanism of submicron carbon spheres

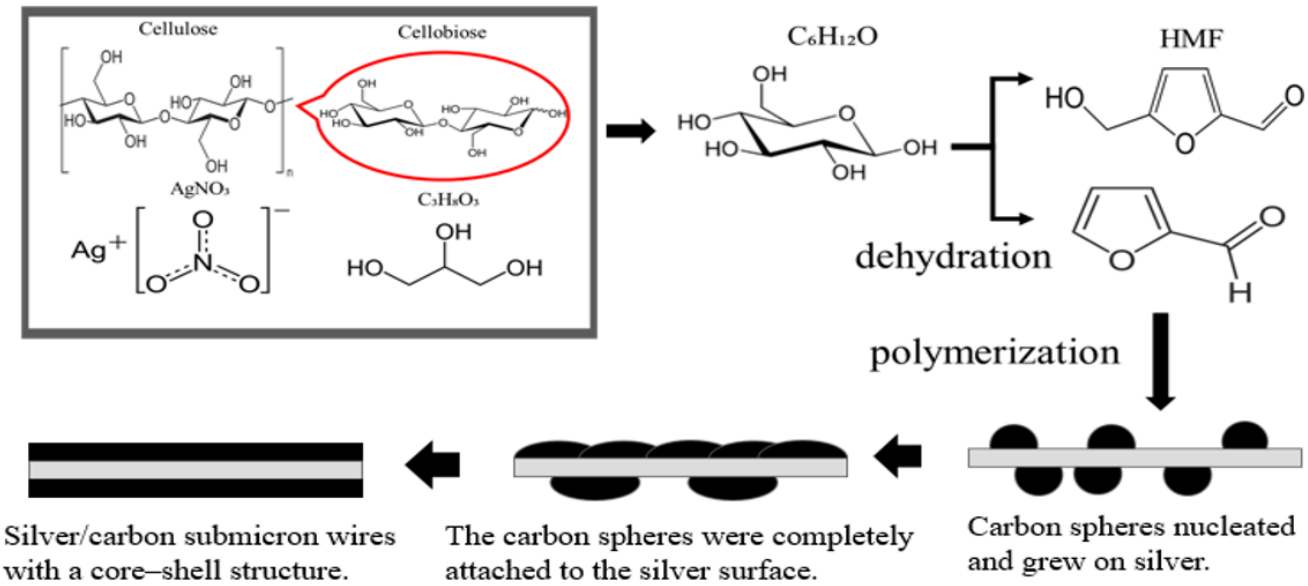


Figure 9

Schematic illustration of the formation mechanism of Ag/C submicron wires

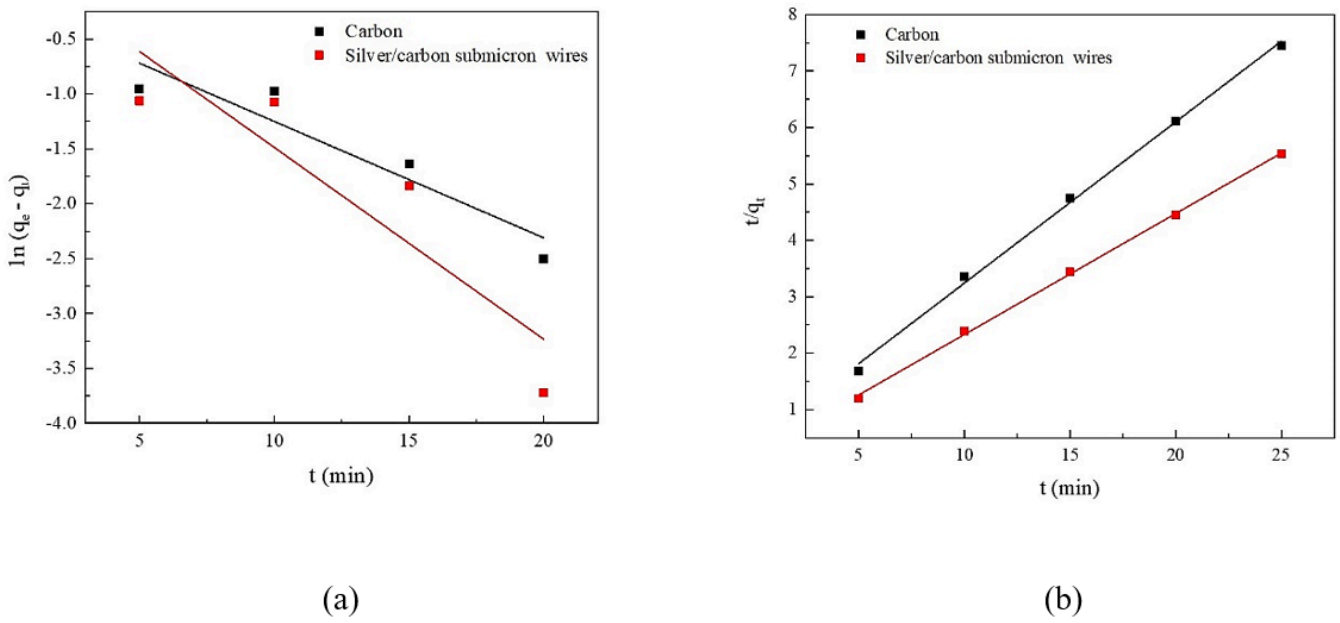


Figure 10

Adsorption kinetics of MB on submicron carbon spheres and Ag/C submicron wires. (a) Pseudo-first-order kinetic model plots, and (b) Pseudo-second-order kinetic model plots